

# Behaviour of the Dam-Break Problem for the Serre Equations

Jordan Pitt,<sup>1</sup>  
Christopher Zoppou,<sup>1</sup>  
Stephen G. Roberts,<sup>1</sup>

## ABSTRACT

**Keywords:** dispersive waves, conservation laws, Serre equation, finite volume method, finite difference method

## INTRODUCTION

## SERRE EQUATIONS

The Serre equations can be derived as an approximation to the full Euler equations by depth integration similar to (Su and Gardner 1969). They can also be seen as an asymptotic expansion to the Euler equations as well (Lannes and Bonneton 2009). The former is more consistent with the perspective from which numerical methods will be developed while the latter indicates the appropriate regions in which to use these equations as a model for fluid flow. The set up of the scenario under which the Serre approximation is made consists of a two dimensional  $\mathbf{x} = (x, z)$  fluid over a bottom topography as in Figure 1 acting under gravity. Consider a fluid particle at depth  $\xi(\mathbf{x}, t) = z - h(x, t) - z_b(x)$  below the water surface, see Figure 1. Where the water depth is  $h(x, t)$  and  $z_b(x)$  is the bed elevation. The fluid particle is subject to the pressure,  $p(\mathbf{x}, t)$  and gravitational acceleration,  $\mathbf{g} = (0, g)^T$  and has a velocity  $\mathbf{u} = (u(\mathbf{x}, t), w(\mathbf{x}, t))$ , where  $u(\mathbf{x}, t)$  is the velocity in the  $x$ -coordinate and  $w(\mathbf{x}, t)$  is the velocity in the  $z$ -coordinate and  $t$  is time. Assuming that  $z_b(x)$  is constant the Serre equations read (Li et al. 2014)

$$\frac{\partial h}{\partial t} + \frac{\partial(\bar{u}h)}{\partial x} = 0 \quad (1a)$$

---

<sup>1</sup>Mathematical Sciences Institute, Australian National University, Canberra, ACT 0200, Australia, E-mail: Jordan.Pitt@anu.edu.au. The work undertaken by the first author was supported financially by an Australian National University Scholarship.

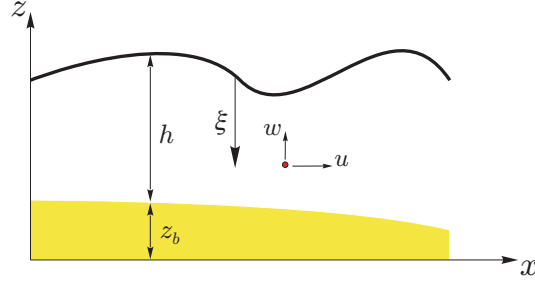


FIG. 1: The notation used for one-dimensional flow governed by the Serre equation.

$$\underbrace{\frac{\partial(\bar{u}h)}{\partial t} + \frac{\partial}{\partial x} \left( \bar{u}^2 h + \frac{gh^2}{2} \right)}_{\text{Shallow Water Wave Equations}} + \underbrace{\frac{\partial}{\partial x} \left( \frac{h^3}{3} \left[ \frac{\partial \bar{u}}{\partial x} \frac{\partial \bar{u}}{\partial x} - \bar{u} \frac{\partial^2 \bar{u}}{\partial x^2} - \frac{\partial^2 \bar{u}}{\partial x \partial t} \right] \right)}_{\text{Dispersion Terms}} = 0. \quad (1b)$$

Serre Equations

Where  $\bar{u}$  means the average of  $u$  over the depth of water.

## FINITE DIFFERENCE AND LAX WENDROFF

This method was used in El et al. (2006) for the Serre equations. It consists of a lax-wendroff update for  $h$  and a spatio-temporal second order approximation to  $[\ ]$  which results in a fully second-order method. To make this method precise it will be presented here in sufficient replicable detail.

Note that  $[\ ]$  is in conservative law form for  $h$  where the Jacobian is  $u$ , where the bar has been dropped to simplify the notation. Thus assuming a fixed resolution discretisation for space and time which will be represented as follows  $q_i^n = q(x_i, t^n)$  for some quantity  $q$  the lax-wendroff update for  $h$  obtained is

$$h_i^{n+1} = h_i^n - \frac{\Delta t}{2\Delta x} ((uh)_{i+1}^n - (uh)_{i-1}^n) + \frac{\Delta t^2}{2\Delta x^2} \left( \frac{u_{i+1}^n - u_i^n}{2} ((uh)_{i+1}^n - (uh)_i^n) - \frac{u_i^n - u_{i-1}^n}{2} ((uh)_i^n - (uh)_{i-1}^n) \right) \quad (2)$$

To get a second-order approximation to  $[\ ]$  is built by first expanding all the derivatives out and making use of the continuity equation  $[\ ]$ , this results in:

$$h \frac{\partial u}{\partial t} + X - h^2 \frac{\partial^2 u}{\partial x \partial t} - \frac{h^3}{3} \frac{\partial^3 u}{\partial x^2 \partial t} = 0 \quad (3a)$$

37 where  $X$  contains only spatial derivatives and is

$$38 \quad X = uh \frac{\partial u}{\partial x} + gh \frac{\partial h}{\partial x} + h^2 \frac{\partial u}{\partial x} \frac{\partial u}{\partial x} + \frac{h^3}{3} \frac{\partial u}{\partial x} \frac{\partial^2 u}{\partial x^2} - h^2 u \frac{\partial^2 u}{\partial x^2} - \frac{h^3}{3} u \frac{\partial^3 u}{\partial x^3}. \quad (3b)$$

40 Then taking second-order approximations to the time derivatives for [] gives

$$41 \quad h^n \frac{u^{n+1} - u^{n-1}}{2\Delta t} + X^n - (h^n)^2 \frac{\left(\frac{\partial u}{\partial x}\right)^{n+1} - \left(\frac{\partial u}{\partial x}\right)^{n-1}}{2\Delta t} - \frac{(h^n)^3}{3} \frac{\left(\frac{\partial^2 u}{\partial x^2}\right)^{n+1} - \left(\frac{\partial^2 u}{\partial x^2}\right)^{n-1}}{2\Delta t} = 0 \quad (4)$$

$$44 \quad h^n (u^{n+1} - u^{n-1}) + 2\Delta t X^n - (h^n)^2 \left( \left(\frac{\partial u}{\partial x}\right)^{n+1} - \left(\frac{\partial u}{\partial x}\right)^{n-1} \right) - \frac{(h^n)^3}{3} \left( \left(\frac{\partial^2 u}{\partial x^2}\right)^{n+1} - \left(\frac{\partial^2 u}{\partial x^2}\right)^{n-1} \right) = 0 \quad (5)$$

$$46 \quad h^n u^{n+1} - (h^n)^2 \left(\frac{\partial u}{\partial x}\right)^{n+1} - \frac{(h^n)^3}{3} \left(\frac{\partial^2 u}{\partial x^2}\right)^{n+1} + 2\Delta t X^n - h^n u^{n-1} + (h^n)^2 \left(\frac{\partial u}{\partial x}\right)^{n-1} + \frac{(h^n)^3}{3} \left(\frac{\partial^2 u}{\partial x^2}\right)^{n-1} = 0 \quad (6)$$

48 Let

$$49 \quad Y^n = 2\Delta t X^n - h^n u^{n-1} + (h^n)^2 \left(\frac{\partial u}{\partial x}\right)^{n-1} + \frac{(h^n)^3}{3} \left(\frac{\partial^2 u}{\partial x^2}\right)^{n-1} \quad (7)$$

51 Taking second-order approximations to the spatial derivatives gives

$$52 \quad h_i^n u_i^{n+1} - (h_i^n)^2 \left( \frac{u_{i+1}^{n+1} - u_{i-1}^{n+1}}{2\Delta x} \right) - \frac{(h_i^n)^3}{3} \left( \frac{u_{i+1}^{n+1} - 2u_i^{n+1} + u_{i-1}^{n+1}}{\Delta x^2} \right) = -Y_i^n \quad (8)$$

54 This can be rearranged into a tri-diagonal matrix that updates  $u$  given its current and previous values. So that

$$56 \quad \begin{bmatrix} u_0^{n+1} \\ \vdots \\ u_m^{n+1} \end{bmatrix} = A^{-1} \begin{bmatrix} -Y_0^n \\ \vdots \\ -Y_m^n \end{bmatrix} =: \mathcal{G}_u(\mathbf{u}^n, \mathbf{h}^n, \mathbf{u}^{n-1}, \Delta t).$$

58 Where

$$59 \quad A = \begin{bmatrix} b_0 & c_0 & & & & \\ a_0 & b_1 & c_1 & & & \\ & a_1 & b_2 & c_2 & & \\ & & \ddots & \ddots & \ddots & \\ & & & a_{m-3} & b_{m-2} & c_{m-2} \\ & & & & a_{m-2} & b_{m-1} & c_{m-1} \\ & & & & & a_{m-1} & b_m \end{bmatrix}$$

with

$$a_{i-1} = \frac{(h_i^n)^2}{2\Delta x} \frac{h_{i+1}^n - h_{i-1}^n}{2\Delta x} - \frac{(h_i^n)^3}{3\Delta x^2}, \quad (9a)$$

$$b_i = h_i^n + \frac{2h_i^n}{3\Delta x^2} \quad (9b)$$

and

$$c_i = -\frac{(h_i^n)^2}{2\Delta x} \frac{h_{i+1}^n - h_{i-1}^n}{2\Delta x} - \frac{(h_i^n)^3}{3\Delta x^2}. \quad (9c)$$

61 Lastly the final expression for  $Y_i^n$  is given by:

$$62 \quad Y_i^n = 2\Delta t X_i^n - h_i^n u_i^{n-1} + (h_i^n)^2 \frac{u_{i+1}^{n-1} - u_{i-1}^{n-1}}{2\Delta x} + \frac{(h_i^n)^3}{3} \frac{u_{i+1}^{n-1} - 2u_i^{n-1} + u_{i-1}^{n-1}}{\Delta x^2} \quad (10)$$

$$63 \quad \begin{aligned} Y_i^n = 2\Delta t & \left[ u_i^n h_i^n \frac{u_{i+1}^n - u_{i-1}^n}{2\Delta x} + g h_i^n \frac{h_{i+1}^{n-1} - h_{i-1}^{n-1}}{2\Delta x} + (h_i^n)^2 \left( \frac{u_{i+1}^{n-1} - u_{i-1}^{n-1}}{2\Delta x} \right)^2 \right. \\ & + \frac{(h_i^n)^3}{3} \frac{u_{i+1}^n - u_{i-1}^n}{2\Delta x} \frac{u_{i+1}^n - 2u_i^n + u_{i-1}^n}{\Delta x^2} - (h_i^n)^2 u_i^n \frac{u_{i+1}^n - 2u_i^n + u_{i-1}^n}{\Delta x^2} \\ & \left. - \frac{(h_i^n)^3}{3} u_i^n \frac{u_{j+2}^n - 2u_{j+1}^n + 2u_{j-1}^n - u_{j-2}^n}{2\Delta x^3} \right] \\ & - h_i^n u_i^{n-1} + (h_i^n)^2 \frac{u_{i+1}^{n-1} - u_{i-1}^{n-1}}{2\Delta x} + \frac{(h_i^n)^3}{3} \frac{u_{i+1}^{n-1} - 2u_i^{n-1} + u_{i-1}^{n-1}}{\Delta x^2} \end{aligned} \quad (11)$$

## 66 SECOND ORDER FINITE DIFFERENCE METHOD

67 Above a second order finite difference method for updating  $u$  was given, thus replacing  
68 the numerical method for  $h$  by replacing derivatives with second order finite differences  
69 will give another full finite difference method. From (1a) we expand derivatives and then  
70 approximate them by second order finite differences to give

$$71 \quad \frac{h_i^{n+1} - h_i^{n-1}}{2\Delta t} + u_i^n \frac{h_{i+1}^n - h_{i-1}^n}{2\Delta x} + h_i^n \frac{u_{i+1}^n - u_{i-1}^n}{2\Delta x} = 0 \quad (12)$$

73 After rearranging this to give an update formula one obtains

$$74 \quad h_i^{n+1} = h_i^{n-1} - \Delta t \left( u_i^n \frac{h_{i+1}^n - h_{i-1}^n}{\Delta x} + h_i^n \frac{u_{i+1}^n - u_{i-1}^n}{\Delta x} \right) \quad (13)$$

75

76 Combining this with the update formula for  $u$  [] gives a full finite difference method  
77 for the Serre equations.

## 78 **A HYBRID FINITE DIFFERENCE-VOLUME METHOD FOR SERRE** 79 **EQUATIONS IN CONSERVATIVE FORM**

80 [] also offer another family of numerical methods which can be constructed by first  
81 rearranging the equations into conservative form and then using both a finite difference  
82 and a finite volume method to solve these equations. This paper will make use of the  
83 first-, second- and third-order versions of this method as set out in []. These have been  
84 validated for both smooth and discontinuous problems and their orders of accuracy have  
85 been verified for smooth solutions so they are of particular interest for the comparisons  
86 that will be investigated in this paper.

## 87 **NUMERICAL SIMULATIONS**

88 In this section the methods introduced in this paper will be validated by using them  
89 to approximate an analytic solution of the Serre equations, this will also be used to verify  
90 their order of accuracy. Then an in depth comparison of using these methods for a smooth  
91 approximation to the discontinuous dam break problem will be provided to investigate the  
92 behaviour of these equations in the presence of discontinuities. This is a problem that so  
93 far has only received a proper treatment in (El et al. 2006), with other research giving only  
94 a cursory look into the topic.

## 95 **SOLITON**

96 Currently cnoidal waves are the only family of analytic solutions to the Serre equa-  
97 tions (Carter and Cienfuegos 2011). Solitons are a particular instance of cnoidal waves  
98 that travel without deformation and have been used to verify the convergence rates of the  
99 described methods in this paper.

100 For the Serre equations the solitons have the following form

$$101 \quad h(x, t) = a_0 + a_1 \operatorname{sech}^2(\kappa(x - ct)), \quad (14a)$$

102  
103

$$104 \quad u(x, t) = c \left( 1 - \frac{a_0}{h(x, t)} \right), \quad (14b)$$

105

106

107

108

$$\kappa = \frac{\sqrt{3a_1}}{2a_0 \sqrt{a_0 + a_1}} \quad (14c)$$

109 and

110

$$c = \sqrt{g(a_0 + a_1)} \quad (14d)$$

112 where  $a_0$  and  $a_1$  are input parameters that determine the depth of the quiescent water and  
 113 the maximum height of the soliton above that respectively. In the simulation  $a_0 = 10m$ ,  
 114  $a_1 = 1m$  for  $x \in [-500m, 1500m]$  and  $t \in [0s, 100s]$ . With  $\Delta t = 0.01\Delta x$  which satisfies []  
 115 and  $\theta = 1.2$  for the second-order finite difference-volume method.

## 116 SMOOTHED DAM-BREAK

117 The discontinuous dam-break problem can be approximated by a smooth function us-  
 118 ing the hyperbolic tangent function. Such an approximation will be called a smoothed  
 119 dam-break problem and will be defined as such

$$h(x, 0) = h_0 + \frac{h_1 - h_0}{2} (1 + \tanh(\alpha(x_0 - x))), \quad (15a)$$

122

123

$$u(x, 0) = 0.0m/s. \quad (15b)$$

125 Where  $a$  is given and controls the width of the transition between the two dam-break  
 126 heights of  $h_0$  and  $h_1$ . For large  $\alpha$  the width is small and vice versa. For a fixed  $\Delta x$  there  
 127 are large enough  $\alpha$  values such that the transition width is zero. This experiment was run  
 128 for both of the methods described in this paper and the 3 different order finite difference-  
 129 volume methods described in []. In this particular simulation  $h_0 = 1.0m$ ,  $h_1 = 1.8m$  on  
 130  $x \in [0m, 1000m]$  for  $t \in [0s, 30s]$  with  $x_0 = 500m$ . The simulations were run changing  
 131 both  $\Delta x$  and  $\alpha$  and for stability  $\Delta t = 0.01\Delta x$  while for the second-order finite volume  
 132 method  $\theta = 1.2$ . Since this experiment involves a very large amount of data the analysis  
 133 will be broken up into three sections: decreasing  $\Delta x$ , increasing  $\alpha$  and finally differences  
 134 between the methods.

## 135 Changing $\Delta x$

136 Decreasing  $\Delta x$  allows the numerical method to better approximate the analytic solution  
 137 to the equations. So for our valid [] numerical methods it would be expected that smaller  
 138  $\Delta x$ 's provide a closer approximation to the analytic solution This was demonstrated for  
 139 smooth problems [] above.

140 In this comparison we pick an  $\alpha$  and a method and investigate the result of decreasing  
141  $\Delta x$ . Because the smoothness of the initial conditions depends on both  $\Delta x$  and  $\alpha$  one must  
142 be careful that the initial conditions do not change from discontinuous to smooth as  $\Delta x$  is  
143 altered as then we are no longer comparing smooth problems. This is of particular impor-  
144 tance for the two finite difference methods as they do not correctly handle discontinuos  
145 initial conditions. []

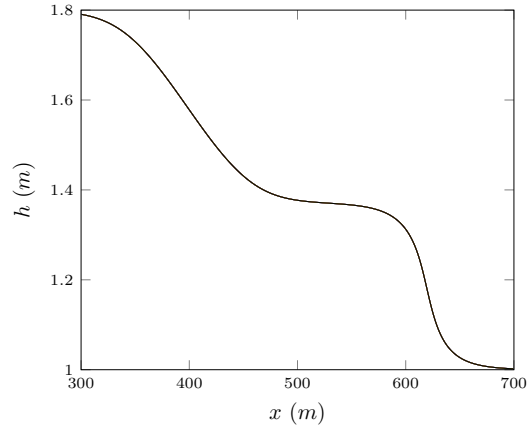
146 The first and most important observation is that there are four types of behaviour as  
147  $\Delta x \rightarrow 0$  of the problem depending on the  $\alpha$  and the numerical method. It was found  
148 that the second- and third-order methods had similar  $\alpha$  ranges determining the trending  
149 behaviour while the first-order had very different ranges, because of this large difference  
150 the term higher-order will be used to refer to all second- and third- order methods. Also  
151 for the purposes of simplicity these scenario's will be demonstrated by solutions of the  
152 FDVM as they are better for illustrative purposes. The four scenarios are identified by the  
153 behaviour of the solutions when  $\Delta x$  is small and they correspond to different results in the  
154 literature.

155 The first behaviour which will be referred to as the non-oscillatory scenario has such  
156 smooth initial conditions that there are no introduced oscillations. This scenario ends at  
157  $\alpha = 0.025$  and should in theory extend down to the trivial  $\alpha = 0$ , in these ranges the  
158 smoothed dam-break problem is a very poor approximation to the dam-break problem.  
159 This behaviour was observed for all methods when  $\alpha = 0.025$  and an example case for the  
160 third-order method is plotted in Figure 2. This example demonstrates rapid convergence  
161 with all the solutions being graphically identical. This scenario resembles the solution of  
162 the shallow water wave equations in that it contains only a rarefaction and a shock with no  
163 dispersion.

164 The second will be referred to as the flat scenario due to the presence of a con-  
165 stant height state between the oscillations at the shock and rarefaction fan. This scenario  
166 emerges at  $\alpha = 0.05$  and continues to  $\alpha = 1$  for the higher-order methods and occurs from  
167  $\alpha = 0.05$  to  $\alpha = 1000$  for the first-order method (so far). This scenario corresponds to the  
168 results presented by Le Métayer et al. (2010) and Mitsotakis et al. (2014).

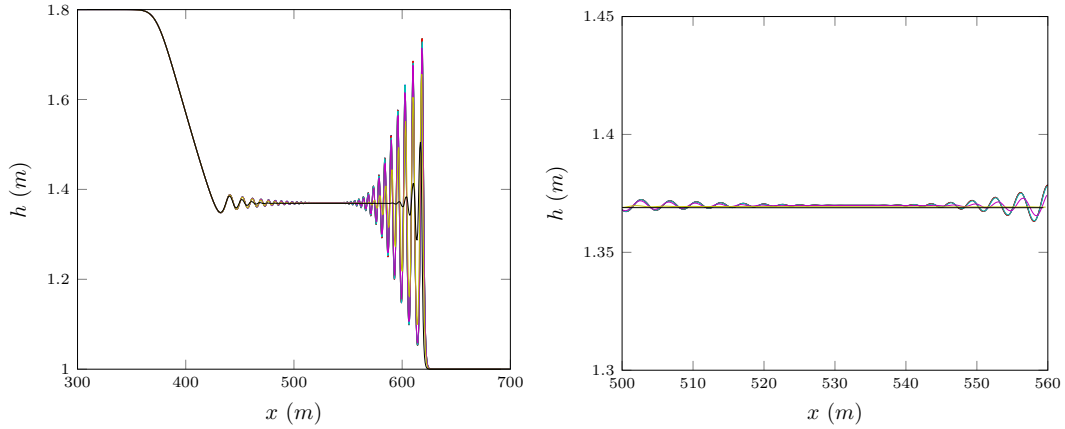
169 An example plot demonstrating this scenario for the third-order method with  $\alpha = 0.5$   
170 can be seen in Figure 3. As  $\Delta x$  decreases the solutions converge which is sensible since for  
171 the  $\Delta x$  in Figure [] the initial conditions are smooth as can be seen in Figure [] and these  
172 methods have been verified for smooth problems. So that by  $\Delta x = 10/2^8$  the solutions for  
173 higher  $\Delta x$  are graphically identical.

174 The third scenario will be referred to as the contact discontinuity scenario due to the  
175 use of that term to describe it by El et al. (2006). For the higher-order methods it occurs at  
176  $\alpha = 2.5$  and so far has not occurred for the first order method[]. The contact discontinuity  
177 scenarios main feature is that the oscillations from the rarefaction fan and the shock decay



(a)

FIG. 2: Smooth dam break problem for o3 [] with  $\alpha = 0.025$  for  $\Delta x = 10/2^{10}$  (blue),  $\Delta x = 10/2^9$  (green),  $\Delta x = 10/2^8$  (red),  $\Delta x = 10/2^7$  (cyan),  $\Delta x = 10/2^6$  (magenta),  $\Delta x = 10/2^5$  (yellow),  $\Delta x = 10/2^4$  (black)



(a)

(b)

FIG. 3: Smooth dam break problem for o3 [] with  $\alpha = 0.5$  for  $\Delta x = 10/2^{10}$  (blue),  $\Delta x = 10/2^9$  (green),  $\Delta x = 10/2^8$  (red),  $\Delta x = 10/2^7$  (cyan),  $\Delta x = 10/2^6$  (magenta),  $\Delta x = 10/2^5$  (yellow),  $\Delta x = 10/2^4$  (black)



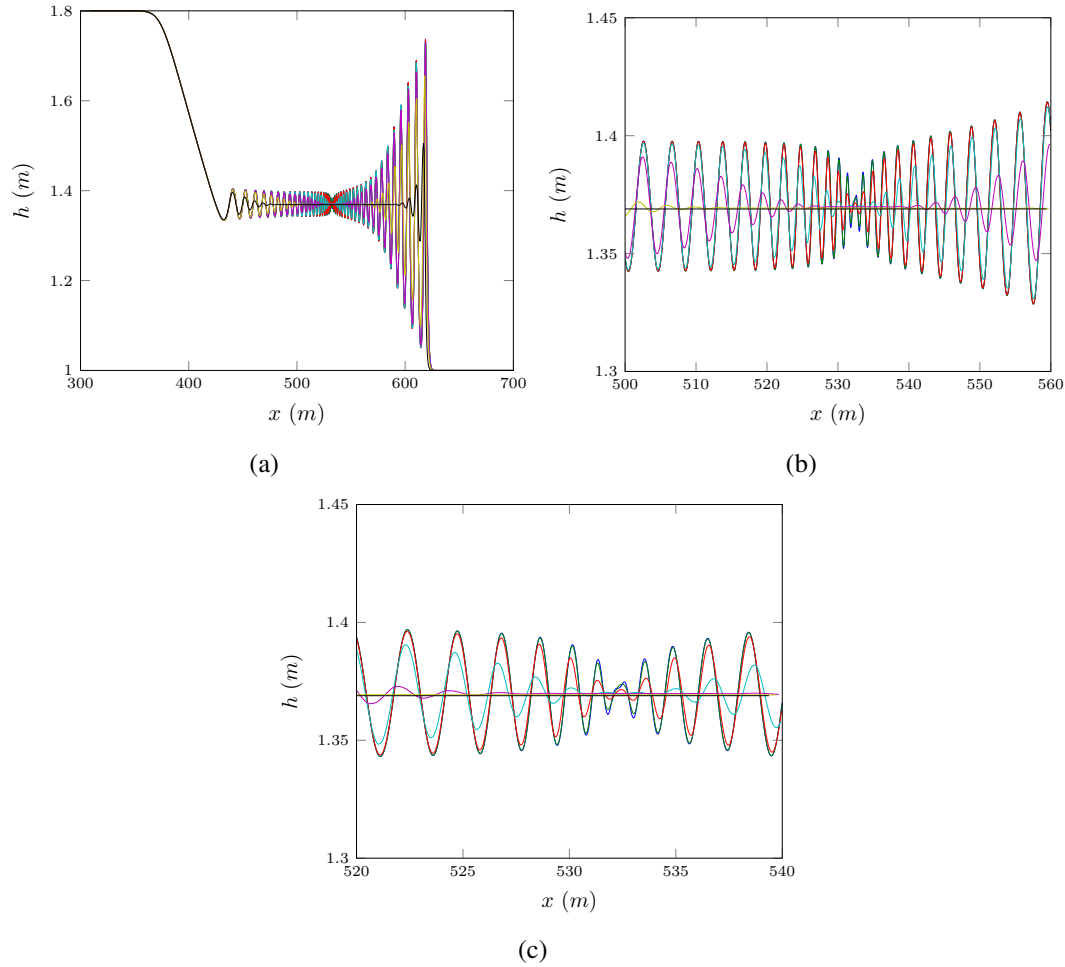


FIG. 4: Smooth dam break problem for o3 [] with  $\alpha = 2.5$  for  $\Delta x = 10/2^{10}$  (blue),  $\Delta x = 10/2^9$  (green),  $\Delta x = 10/2^8$  (red),  $\Delta x = 10/2^7$  (cyan),  $\Delta x = 10/2^6$  (magenta),  $\Delta x = 10/2^5$  (yellow),  $\Delta x = 10/2^4$  (black)

and appear to meet at a point as can be seen in Figure 4. For the experiments performed this doesn't appear to be an actual centre point but rather that the oscillations decay so quickly around the 'contact discontinuity' that it appears to be the case. All the higher order methods so far have not shown a converged solution as  $\Delta x$  decreases. However it does appear that convergence is likely with the solutions getting closer together.

The fourth scenario will be referred to as the bump scenario due to the oscillations no longer decaying down towards a point but rather growing around where the contact discontinuity was in the previous scenario as can be seen in Figure 5. This behaviour

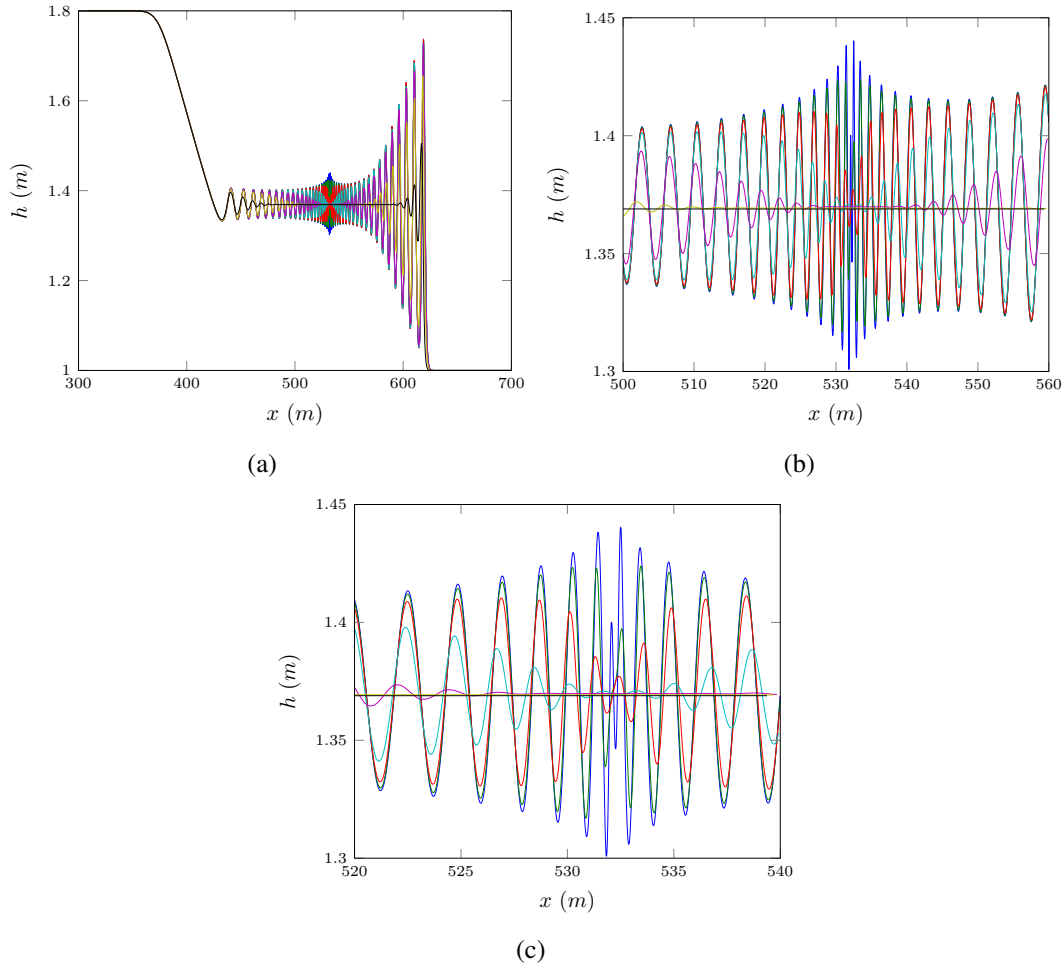


FIG. 5: Smooth dam break problem for o3 [] with  $\alpha = 1000.0$  for  $\Delta x = 10/2^{10}$  (blue),  $\Delta x = 10/2^9$  (green),  $\Delta x = 10/2^8$  (red),  $\Delta x = 10/2^7$  (cyan),  $\Delta x = 10/2^6$  (magenta),  $\Delta x = 10/2^7$  (yellow),  $\Delta x = 10/2^8$  (black)

has hitherto not been presented and is certainly not an expected result. There are some important observations, changing  $\alpha$  does increase the height of the bump for the lowest resolution methods although after [] increasing  $\alpha$  has no effect[huh?]. The behaviour of these solutions in Figure 5 do not clearly show convergence, although it doesn't appear that there is a rapid divergence which suggests that this behaviour is not unstable. Also the lack of convergence is only around the contact discontinuity with other parts of the solution showing convergence.

All of the scenarios described above and displayed using the higher-order FDVM also

occur for the FDM, however because finite differences cannot properly handle discontinuities this is a little more subtle. Firstly, since for each  $\alpha$  there is a  $\Delta x$  such that for larger  $\Delta x$  the smooth dam break problem is no longer smooth enough for a finite difference approximation to be appropriate. This becomes a problem for the contact discontinuity and bump scenarios since they require higher  $\alpha$  and are thus more discontinuous to begin with. The result of this are non-physical looking oscillations for large  $\Delta x$  values that were not replicated by the FDVM and thus can be attributed to this flaw of FDM as in Figure [].

Overall there were two types of trending behaviours as  $\Delta x$  was decreased one for the FDM and another for the FDVM. FDM decreased the number of oscillations in the solution as in Figure [], while FDVM increased the number of oscillations in the solution as can be seen in Figure []. This is explained by Zoppou and Roberts (1996) as the FDM are second order finite difference approximations their errors are dissipative thus introducing oscillatory errors which are most prominent when  $\Delta x$  and therefore the errors are large. While the behaviour of the FDVM is explained by a series of effects [] [TVD, treating things as cell averages, thus flattening things in cells,].

[(verify convergence rates near discontinuities?)

## Changing $\alpha$

Increasing  $\alpha$  allows the initial conditions (8) to approach the dam break problem with  $h_1$  to the left and  $h_0$  to the right centred around  $x_0$ . So it would be expected that as  $\alpha \rightarrow \infty$  that the solution of the smooth dam break problem would approach the corresponding dam break problem. This is the case for numerical methods because for a fixed  $\Delta x$   $\alpha$  can be chosen large enough that (8) is precisely the dam break problem. This can be seen in Figure [] with  $\Delta x =$  where the required  $\alpha$  for this to occur is below 1000 which was the maximum  $\alpha$  value used in these experiments. However, only the FDVM were able to handle such large  $\alpha$ 's because the initial conditions are not smooth enough to allow for stability in the FDM as can be seen in Figure []. While the FDVM handled this quite well and for all  $\Delta x$  tested as  $\alpha$  increased the solutions converged, even though for higher  $\Delta x$  []  $\alpha$  was not large enough to make (8) a jump discontinuity.

This confirms the superiority of the FDVM to handle non smooth initial conditions and the inability of FDM to handle them. Even near discontinuous initial conditions caused problems for the FDM with the introduction of oscillations that were not replicated by the FDVM and appeared to be non-physical. An example of these transitional solutions between the properly smooth initial conditions and the unstable discontinuous ones can be seen in Figure []. [(only compare the models when FD started smooth enough)

For the range of  $\alpha$ 's which are smooth enough for the FDM to be appropriate then as  $\alpha$  increases the number of oscillations increases as well for both the FDM and the FDVM. So that the smoothness of the initial conditions controls the oscillations but this depends on  $\Delta x$  since for a fixed  $\alpha$  the smoothness of the discretised initial conditions depends on

232  $\Delta x$ . [] (relative smoothness, more universal number)

233 It was observed that  $\Delta x$  can be chosen large enough such that increasing  $\alpha$  does not  
234 resolve some of the more complex structure observed for smaller  $\Delta x$  values. This  $\Delta x$   
235 depends on the model most notably for the first-order finite difference-volume scheme this  
236  $\Delta x$  is very small. An example of this for the third-order FDVM scheme can be seen in  
237 Figure [].

## 238 **Comparison of Models**

239 The first-order FDVM was too diffuse and

## 240 **CONCLUSIONS**

## 241 **ACKNOWLEDGEMENTS**

## 242 **REFERENCES**

- 243 Carter, J. D. and Cienfuegos, R. (2011). "Solitary and cnoidal wave solutions of the Serre  
244 equations and their stability." *European Journal of Mechanics B/Fluids*, 30(3), 259–268.
- 245 El, G., Grimshaw, R. H. J., and Smyth, N. F. (2006). "Unsteady undular bores in fully  
246 nonlinear shallow-water theory." *Physics of Fluids*, 18(027104).
- 247 Lannes, D. and Bonneton, P. (2009)." *Physics of Fluids*, 21(1), 16601–16610.
- 248 Le Métayer, O., Gavriluk, S., and Hank, S. (2010). "A numerical scheme for the Green-  
249 Naghdi model." *Journal of Computational Physics*, 229(6), 2034–2045.
- 250 Li, M., Guyenne, P., Li, F., and Xu, L. (2014). "High order well-balanced CDG-FE meth-  
251 ods for shallow water waves by a Green-Naghdi model." *Journal of Computational*  
252 *Physics*, 257, 169–192.
- 253 Mitsotakis, D., Dutykh, D., and Carter, J. (2014). "On the nonlinear dynamics of the  
254 traveling-wave solutions of the serre equations." *arXiv preprint arXiv:1404.6725*.
- 255 Su, C. H. and Gardner, C. S. (1969). "Korteweg-de Vries equation and generalisations.  
256 III. Derivation of the Korteweg-de Vries equation and Burgers equation." *Journal of*  
257 *Mathematical Physics*, 10(3), 536–539.
- 258 Zoppou, C. and Roberts, S. (1996). "Behaviour of finite difference schemes for advection  
259 diffusion equations." *Technical Report Mathematics Research Report No.MRR 062-96*.